2026 IEEE International Conference on Robotics and Automation (ICRA 2026)
June 1-5, 2026. Vienna, Austria

# A Compact Rotary Series Elastic Actuator with Wide Deflection Range and Linear Torque Response for pHRI Applications

Mohamed T. Eraky, Andy Li, Biruk A. Gebre, Kishore Pochiraju, Damiano Zanotto*

***Abstract*— This paper presents the design and characterization of a new series elastic actuator (SEA) for physical human-robot interaction (pHRI) featuring a compact spring mechanism. The spring mechanism consists of ten compression springs, fitted on output rotors and arranged in a curved formation. The compression springs are enclosed in spring chambers featured in input rotors. This design reduces frictional losses and enables all springs to bear load bidirectionally with minimal preload relative to conventional designs that rely on antagonistic spring arrangements, thereby enhancing deflection range and torque capacity. We introduce the SEA design and experimentally characterize the passive torque-deflection curve and the closed-loop torque tracking bandwidth. Bench testing demonstrates a torque capacity of 18 Nm and a maximum stiffness of 43.8 Nm/rad. As a representative application, the SEA is integrated into an ankle exoskeleton, with the spring mechanism co-located at the ankle joint. Treadmill walking tests with the exoskeleton indicate good torque tracking performance, with a root-mean-square error of 1.48 Nm when applying 12% assistance, corresponding to a peak torque of 17.6 Nm.**

***Index Terms*— Series elastic actuator (SEA), bidirectional torsional spring, actuator design, physical human-robot interaction, wearable robotics.**

## I. Introduction

Series Elastic Actuators (SEAs) are commonly used in robots designed for physical human-robot interaction (pHRI), including humanoid robots [1], service robots [2], and those developed for assistive [3] and rehabilitation [4]. Key advantages of integrating a spring element in series with the actuation system include precise control of interaction forces, backdrivability, and enhanced operational safety by decoupling a device's end effector from motor inertia [5]. The elastic element is a critical component of an SEA, as it determines its range of actuation and torque resolution, and affects its closed-loop bandwidth [3]. A compliant spring allows for accurate torque feedback from displacement measurements. However, higher compliance necessitates larger spring deformations to achieve large torques, such as those required in rehabilitation and assistive robots [6]. Therefore, designing an elastic element requires a trade-off between compliance and torque capacity, and developing compliant, compact, and lightweight SEAs with high torque capabilities remains a challenge [7].

Several research groups have focused on balancing compactness, torque capacity, and passive deflection range through monolithic torsional springs [8]. Designs featuring a monolithic spring with one or more spiral arms connecting a center bore to an outer rim enable a wide stiffness range but offer limited passive deflection [6], [9]–[16]. Recent two-element designs use equally spaced cantilever beams, with one end allowed to rotate at the interface with a camshaft, and the other end fixed to a rim [8]. This method improves the energy density of monolithic structures by enabling larger deformations ($\approx$12°). However, sliding contacts between the outer rim and camshaft introduce hysteresis in the torque–deflection response [8].

An alternative SEA architecture relies on arrays of compression springs arranged in antagonistic pairs within prismatic configurations [17]–[19] (Fig. 1-a). While compact, this arrangement typically produces non-linear stiffness. Improved linearity can be achieved using tensile spring arrays, though at the expense of torque capacity [20], [21]. In either case, the initial preload in the antagonistic pairs constrains the allowable deflection range, limiting the SEA's passive capacity [18]. A curved spring topology (Fig. 1-b) was proposed in [22] to achieve linear stiffness within a compact form factor. However, like prismatic layouts, the antagonistic arc configuration limits the passive deformation range based on the required spring preload. Because displacement of one spring necessitates a reciprocal displacement in its pair, the preload must be centered between the spring's maximum compression and its free length to maximize the bidirectional deflection range.

In this paper, we introduce the *Elastic Spinners*, a novel SEA spring that employs linear compression springs arranged in a curved formation on two coaxial, rigidly connected output rotors. The output rotors, implemented as thin plates, rotate relative to an input rotor assembly to concurrently deflect all springs within their respective chambers in the same direction and by an equal amount. This architecture minimizes sliding friction and enables all springs to bear load bidirectionally with minimal required preload. As a result, the mechanism achieves high torque capacity with low hysteresis, a linear bidirectional torque–deflection response, and an extended deflection range.

The remainder of this paper is structured as follows. The design of Elastic Spinners is presented in Section II, while its passive stiffness response is analyzed in Section III. Sec-

*Corresponding author: (dzanotto@stevens.edu).

This work was supported by the U.S. National Science Foundation under Grant CMMI-1944203 and by the U.S. Department of Defense, through the Peer Reviewed Orthopaedic Research Program (PRORP), under Award No. W81XWH-22-1-0193. Opinions, interpretations, conclusions, and recommendations are those of the authors and are not necessarily endorsed by the U.S. Department of Defense.

MTE, AL and DZ are with the Wearable Robotic Systems Lab., Stevens Inst. of Technology, Hoboken, NJ 07030, USA.

BAG and KP are with the PROOF Lab., Stevens Inst. of Technology, Hoboken, NJ 07030, USA.

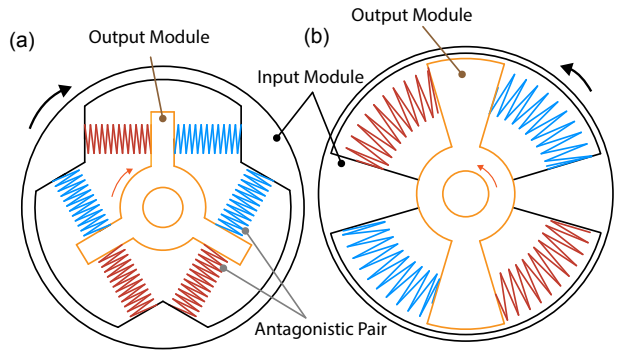


Fig. 1. Examples of SEA spring arrangements previously presented in the literature featuring antagonistic spring pairs: **(a)** conventional compression springs; and **(b)** curved compression springs.

tion IV introduces a SEA integrating Elastic Spinners, and its dynamic characterization. Section V discusses implications and concludes the paper.

## II. Design of Elastic Spinners

### A. Design Overview

As shown in Fig. 2-a,c, Elastic Spinners consists of an input rotor assembly and a pair of rigidly-connected output rotors housed within the input rotor assembly. The input rotor assembly comprises a middle plate and two cover plates featuring complementary cutouts that form spring chambers, providing sufficient clearance to prevent sliding contact between the springs and the chamber walls during operation (Fig. 2-b). The output rotors are mounted on an output shaft supported by bearings with extended inner rings, enabling them to rotate with respect to the input rotor. Three auxiliary torque links (Fig. 2-a) are used to transmit the generated torque. Each output rotor is machined as a thin plate and featured with five arc cutouts arranged circumferentially. The arc length of these cutouts ensures sufficient preload (Sec. II-B). Clearance gaps in the arc cutouts accommodate spring buckling during deformation (Fig. 2-d,e). Together with the lateral cutouts in the spring chambers, these clearance gaps eliminate sliding contacts across the springs' deflection range. As the output rotors rotate relative to the input rotor assembly, all springs deflect by the same amount, generating a reaction torque on the output rotors, which is transmitted to the torque links and output shaft.

The output shaft is made of stainless steel (AISI 303) and the torque links are made of alloy steel. The output rotors are made of aerospace-grade aluminum alloy (7075-T6), chosen for its high strength-to-weight ratio and light weight, while the input rotor assembly is made of 6061 aluminum alloy. The design of the output rotors was refined through iterative finite element analysis to achieve a fatigue life of 133,732 cycles (top-right inset in Fig. 2-c). Considering the intended application in an ankle exoskeleton for gait rehabilitation (Sec. IV), and a maximal assistance of 18 Nm once per gait cycle, the elastic element would need to be replaced after approximately 50 rehabilitation sessions (assuming a nominal pace of 120 steps per minute and a standard 45-minute PT exercise session), which was deemed appropriate.

### B. Stiffness Model

In this section, the design workflow to obtain an Elastic Spinners with desired stiffness and passive deflection range is presented. The following simplifying assumptions are made: (i) all compression springs are identical; (ii) spring buckling has negligible effect on the linear stiffness response of each spring. Motivated by the application to a powered ankle exoskeleton for gait rehabilitation (Fig. 2-f), we set the design peak torque to $\tau_{\max} = 18$ Nm and its deformation range to $\Delta\theta_{\max} = \pm 24^{\circ}$. The selected $\tau_{\max}$ corresponds to approximately 15% of the peak ankle plantarflexion torque for a 75 kg adult male walking at normal pace, while $\Delta\theta_{\max}$ exceeds the expected plantar- and dorsi-flexion range during walking [23]. To simplify the low-level control of the SEA, a linear torque-deflection response in the elastic element is desirable [6]. The most compliant linear elastic element that achieves both requirements has a target passive torsional stiffness $K_{\text{ES}} = 42.97$ Nm/rad. To achieve the target $K_{\text{ES}}$ and $\Delta\theta_{\max}$ within a compact design, we rely on a set of $N$ identical helical compression springs arranged circumferentially on the output rotor of the elastic element. The passive torsional stiffness of each spring is estimated using the model of an arc helical spring with circular cross-section subjected to circumferential force [24]

$$K_{ac} = \frac{Gd^4R^2}{8D^3n}, \tag{1}$$

where $D$ and $d$ are the average diameter of the spring and the diameter of the spring wire, respectively, $R$ is the radius of the circumference along which the coil axis of the helical spring lies, $n$ is the number of active coils, and $G$ is the shear modulus. Because all springs in the output rotors act in parallel, the desired torsional stiffness for each spring is

$$K_{ac} = \frac{K_{\text{ES}}}{N} \tag{2}$$

Conventional linear compression springs were chosen over arc springs, as they are widely available and avoid reliance on specialized components. Comparing (1) to Wahl's model of axially-loaded cylindrical helical spring [25], we obtain the design linear stiffness $K_{cc}$ for each compression spring:

$$K_{cc} = \frac{K_{ac}}{R^2} \tag{3}$$

The total elastic torque is

$$\tau = NK_{cc}R^2\Delta\theta, \tag{4}$$

where $\Delta\theta$ is the deflection angle. To enable a maximum deflection angle $\Delta\theta_{\max}$, the free length $S_f$ and the solid length $S_l$ of each compression spring must satisfy

$$(S_f - S_l) \geq \left(R - \frac{D}{2}\right)\Delta\theta_{\max} + \xi, \tag{5}$$

where $\xi$ indicates the spring preload. The mechanical properties of the selected spring are summarized in Tab. I.

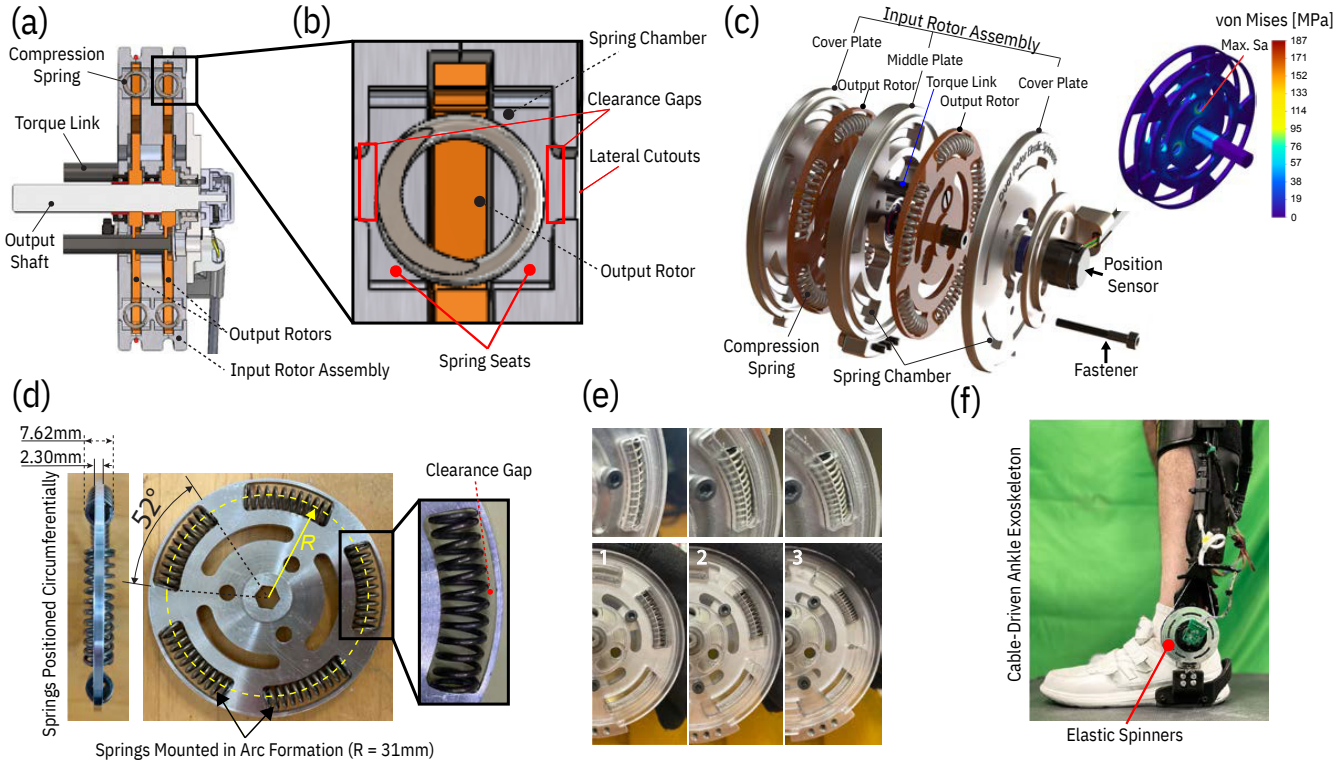


Fig. 2. Design of *Elastic Spinners*: (a) Sectional view illustrating the output rotors enclosed within the input rotor assembly; (b) Sectional view of a spring chamber; (c) Exploded view, showing the components of Elastic Spinners; (d) Springs installed circumferentially on an output rotor with preload; (e) Progressive deformation of a compression spring (bottom row), showing the clearance gap between the spring coils and the cover plate (top row); (f) Elastic Spinners mounted on a powered ankle exoskeleton.

Considering the shear modulus of AISI 316 Stainless Steel ($G$ =74.23 GPa), and a radius $R = 31$ mm to achieve a compact design suitable for wearable applications, the calculated spring torsional stiffness is 4.6 Nm/rad. Thus, a dual-rotor design with 5 springs mounted on each output rotor results in an overall calculated stiffness of 46 Nm/rad, which is a good approximation of the target value $K_{\text{ES}}$. Furthermore, (5) indicates that the selected spring can achieve $\Delta\theta_{\max}$ with a small preload of $\xi \approx 3-4$ mm. This represents a two- to three-fold reduction compared to the preload required by a conventional curved spring antagonistic design (Fig. 1-b) featuring the same springs (and therefore yielding the same equivalent stiffness). This minimal preload is sufficient to keep the springs seated against each output rotor and avoid backlash. When combined with a rotor architecture that enables all springs to deflect in the same direction, this reduced preload substantially enhances bidirectional deflection range. The resulting specification of Elastic Spinners are listed in Tab. II.

## III. Passive Stiffness Characterization

Experimental characterization was carried out to measure the passive stiffness of Elastic Spinners. In the test setup (Fig. 3-a), the input rotor assembly was fixed to a stationary frame, while the output shaft was connected to a torque sensor via a flange. The deformation of Elastic Spinners was measured using a position sensor (micro-optical encoder E16, US Digital, USA) with 16384 pulses per revolution. A custom-made data acquisition and conditioning (DAQ) board that includes a 32-bit microcontroller (Teensy 3.5, PJRC, USA), an EtherCAT shield (EasyCAT Pro, AB&T Srl, Italy), and a 12-bit ADC (AD7890ANZ-10, Analog Devices, USA) was connected to a real-time target machine (Unit, Speedgoat

TABLE I
Elastic Spinners' Compression Spring

| | |
|---|---|
| Free Length | 31.75 mm |
| Compressed Length @Maximum Load | 12.217 mm |
| Passive Stiffness/Spring Rate | 3654.9 N/m |
| Outer Diameter | 7.62 mm |
| Inner Diameter | 5.54 mm |
| Wire Diameter | 1.04 mm |
| Active Coils (n) | 8 |
| Material | AISI 316 |

TABLE II
Specifications of Elastic Spinners

| | |
|---|---|
| Maximum Diameter | 82 mm |
| Thickness | 18.5 mm |
| Weight | 0.217 kg |
| Measured Passive Stiffness | 43.8 Nm/rad |
| Energy Capacity | 3.8 J |
| Specific Energy | 17.24 J/kg |
| Peak Torque | 18 Nm |
| Max Passive Deflection | $\pm$0.42 rad ($\pm$24°) |

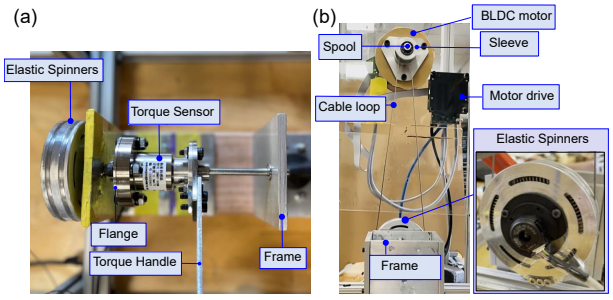


Fig. 3. (a) Test rig used to evaluate the torque-deflection response of Elastic Spinners. (b) Test rig used to evaluate the SEA dynamic response.

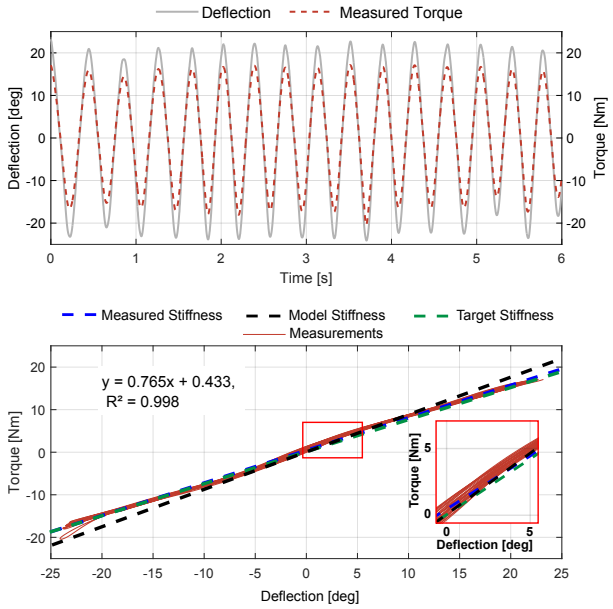


Fig. 4. (a) Applied deflection (left) and corresponding measured torque (right). (b) The passive response of Elastic Spinners is approximately linear over a useful deformation range of ±24 deg (43.8 Nm/rad, 0.765 Nm/deg).

GmbH, Switzerland), allowing data collection from position and torque sensors over EtherCAT bus at 1 kHz.

Using a torque handle connected to the torque sensor, an experimenter applied an approximate sinusoidal trajectory spanning the useful deformation range of Elastic Spinners. Passive stiffness and hysteresis were quantified using data collected from 29 bidirectional loading and unloading cycles.

As shown in Fig. 4, Elastic Spinners meets the desired deformation range of $\pm 24^{\circ}$. The measured stiffness (43.83 Nm/rad, or 0.765 Nm/deg) matches the target value $K_{ES}$ within 2.0% and is only 4.7% lower than the model prediction (Sec. II-B). The average percentage energy loss, estimated over a total of 29 loading/unloading cycles, was 2.87%, indicating minimal hysteresis.

## IV. Dynamic Response Characterization

### A. Experimental Setup

To evaluate the dynamic performance of Elastic Spinners, the elastic element was integrated in a cable-driven SEA (Fig. 3-b). The SEA comprises a brushless DC (BLDC) motor (EC90-flat, 600 W, Maxon Group, Switzerland) with

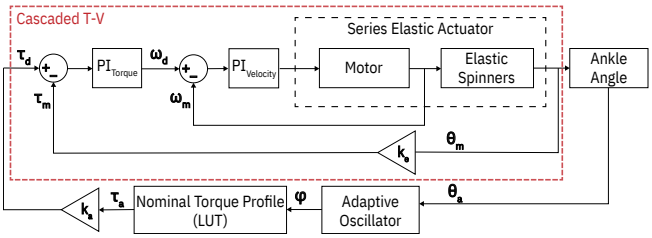


Fig. 5. Cascaded torque–velocity controller (red box) and preliminary assistive controller for the ankle exoskeleton.

integrated encoder (Maxon Mile Encoder) featuring 4096 counts per turn, a motor driver (Maxon EPOS4 Compact 50/15 EtherCAT), as well as the real-time target machine and the DAQ board described in Sec. III. The target machine, the motor driver, and the DAQ communicate over EtherCAT bus at 1kHz. In the testing apparatus, a cable loop connects a threaded spool fixed on the shaft of the BLDC motor to the input rotor assembly. The threaded spool, which is supported by a sleeve to reduce radial loads on the motor shaft, allows for cable winding/unwinding without overlapping. The effective diameters of the input rotor assembly and the threaded spool are 76.6 mm and 12.4 mm, respectively, yielding a transmission ratio of 6:1. A cascaded torque-velocity controller was implemented to enable closed-loop torque control of the SEA for frequency response (Sec. IV-B) and virtual impedance rendering (Sec. IV-C) characterization. The gains for the inner loop velocity controller were auto-tuned using EPOS Studio v3.7, whereas the outer loop gains were tuned manually.

Subsequently, the SEA was installed on the shank module of a cable-driven ankle exoskeleton [26], and a simple assistive controller was implemented for early human testing (Sec. IV-D), based on a fixed ankle torque profile. The ankle plantar- and dorsi-flexion angle, measured using a position sensor fitted at the medial malleolus, was fed to a pool of adaptive frequency oscillators, which continuously estimate the gait phase [27]. The output of the oscillators was aligned with the wearer's initial contacts (heel strikes) using the readings from an in-shoe force sensitive resistor, and fed to a lookup table (LUT) that stores the normative ankle biomechanical moment as a function of the gait phase [23]. The output of the lookup table was then scaled by a fixed assistance level $k_a$ to obtain the desired assistive torque $\tau_d$, as shown in Fig. 5.

### B. Frequency Response

Frequency response analysis was conducted under infinite output impedance conditions (i.e., locked output shaft). To this end, the output shaft and torque links were fixed to a frame (Fig. 3-b) and the input rotor assembly was excited using three chirp signals with torque amplitudes of 6 Nm, 9 Nm, and 12 Nm. Each torque amplitude was swept across frequencies ranging from 0 to 20 Hz. In Fig. 6 (left), a representative chirp torque signal $\tau_{\mathrm{d}}$ with 12 Nm amplitude is shown, along with the measured response $\tau_{\mathrm{m}}$. The transfer function $H_{\mathrm{SEA}}(j\omega) = \frac{\tau_{\mathrm{m}}}{\tau_{\mathrm{d}}}$ was estimated using MATLAB System Identification Toolbox for each applied

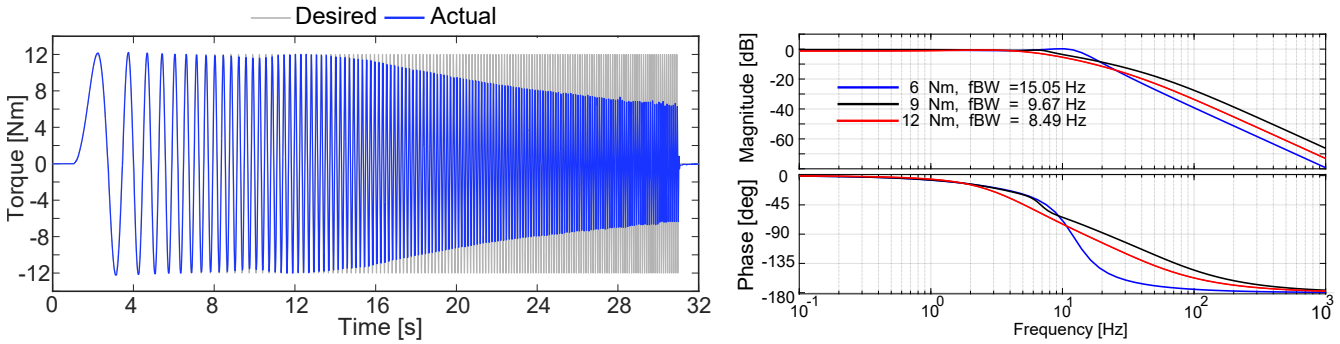


Fig. 6. Closed-loop dynamic response of Elastic Spinners within SEA configuration with locked output shaft. Commanded torque $\tau_{\mathrm{d}}$ (chirp signal, 12 Nm amplitude, 0-20 Hz frequency) and measured response $\tau_{\mathrm{m}}$ (left). Corresponding Bode plots (right) derived by fitting experimental data to LTI transfer functions (4 poles, 2 zeros). The 3dB closed-loop bandwidth $f_{\mathrm{BW}}$ is 15.05 Hz for 6 Nm, 9.67 Hz for 9 Nm, and 8.49 Hz for 12 Nm torque amplitudes. At $f_{\mathrm{BW}}$, the maximum phase lags are $-117.0$ deg, $-90.1$ deg, and $-76.3$ deg, respectively.

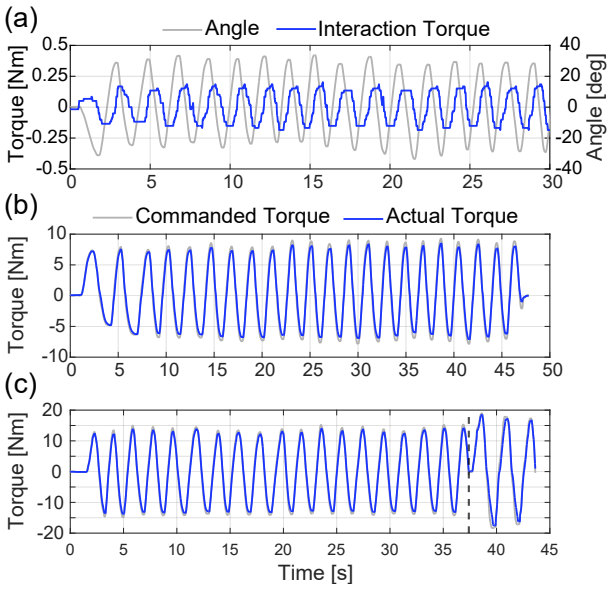


Fig. 7. Virtual stiffness rendering. (a) Virtual spring with null stiffness (zero impedance test). (b) Virtual Spring with one-third of Elastic Spinners' passive stiffness (14.33 Nm/rad). (c) Virtual Spring with two-thirds of Elastic Spinners' passive stiffness (28.67 Nm/rad, left of dashed vertical line) and maximum stiffness (43.8 Nm/rad, right of vertical dashed line).

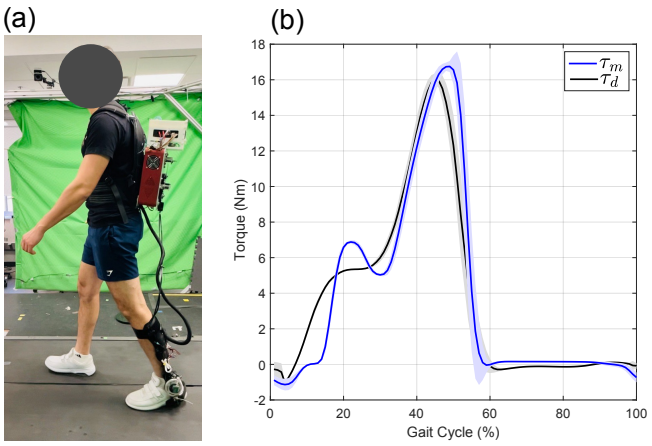


Fig. 8. (a) Healthy individual walking on a treadmill at 1.0 m/s while wearing an ankle exoskeleton fitted with Elastic Spinners, with assistance gain set to $k_a = 12\%$. (b) Average profiles of $\tau_{\mathrm{d}}$ (black) and $\tau_{\mathrm{m}}$ (blue), with colored shades indicating $\pm 1$ SD. The RMSE was 1.48 Nm, indicating very good torque tracking.

torque magnitude. The resulting Bode plots, shown in Fig. 6 (right), indicated a closed-loop bandwidth of 15.05 Hz for 6 Nm, 9.67 Hz for 9 Nm, and 8.49 Hz for 12 Nm of applied torque. The corresponding phase lags at $f_{\mathrm{BW}}$ were $-117.0$ deg, $-90.1$ deg, and $-76.3$ deg, respectively. These results highlight stable closed-loop behavior and very good dynamic performances.

### C. Virtual Impedance Rendering

Tests were performed to evaluate the SEA's ability to render virtual torsional springs with different stiffness values. A torque handle was installed on the output shaft of Elastic Spinners, using the setup shown in Fig. 3-b. During testing, the handle was manually rotated by an experimenter to generate a quasi-periodic perturbation by following a reference signal displayed on a screen, whose frequency and amplitude (0.5 Hz, 30 deg) were selected to ensure a comfortable tracking at different stiffness values. The commanded torque was set to $\tau_{\mathrm{d}} = k_{vs}\,(\theta - \theta_0)$, where $k_{vs}$ is the desired virtual stiffness and $\theta_0 = 0$ rad indicates the unperturbed position of the virtual spring. In the first test (Fig. 7-a), $k_{vs}$ was set to a null value to assess the SEA's transparency [28]. The measured interaction torque $\tau_{\mathrm{m}}$ exhibited small fluctuations that peaked at each inversion of motion within $\pm 0.25$ Nm. The root mean square error (RMSE) was 0.135 Nm, which is approximately 0.75% of Elastic Spinners' torque capacity. In the subsequent tests, the SEA was commanded to render a virtual spring with discrete stiffness values: $k_{vs} = K_{ES}/3$ (Fig. 7-b), $k_{vs} = 2K_{ES}/3$ (Fig. 7-c, left of dashed line), and $k_{vs} = K_{ES}$ (Fig. 7-c, right of dashed line). The RMSE was 0.704 Nm, 0.985 Nm, and 2.138 Nm for the three stiffness values, respectively. Overall, these values suggest that the system was able to render a wide range of stiffness values, with good fidelity, across its allowable range.

### D. Assisted walking

An able-bodied individual (31 year old male, 175 cm height, 77 kg weight) walked on a treadmill at 1.0 m/s (Fig. 8-a). The exoskeleton was controlled in assistive mode,

TABLE III
COMPARISON OF DIFFERENT DESIGNS TORSIONAL SPRINGS

| Reference | Elastic Element Type | Stiffness (Nm/rad) | Max. Torque (Nm) | Passive deflection (deg) | Weight (g) | D/T (mm) |
|---|---|---|---|---|---|---|
| Zhao et al. [21] | Spring array (compression) | 64.74 | 11.3 | $\pm$ 10 | 850 | 96/- |
| Lv et al. [22] | Curved springs | 23.76 | - | - | - | -/- |
| Toubar et al. [18] | Spring array (compression) | 17.2/36.2/54.4 | 45 (clutch maximum) | $\pm$4.5 | - | 140/- |
| Tiseni et al. [20] | Springs array (tension) | 70.4 | 7.99 | $\pm$12.7 | - | 130/- |
| Tsagarakis et al. [17] | Springs array (compression) | Modulated Stiffness | 40 | $\pm$10.3 | 520 | 70/80 |
| Bons et al. [8] | Two-element monolithic | 150 (Average) | - | $\pm$12.6 | 57.3 | 67/4.5 |
| Carpino et al. [6] | Monolithic | 98 | 7.68 | $\pm$4.47 | 61.5 | 85/3 |
| **This work** | Spring array (compression) | 43.8 | 18 | $\pm$24 | 200 | 82/18.5 |

with $k_a = 12\%$. Figure 8-b shows the average profiles of $\tau_{\mathrm{d}}$ and $\tau_{\mathrm{m}}$. The average per-stride peak torque was 17.6 Nm, while the RMSE was $1.48$ Nm, corresponding to approximately 8% of the peak torque, likely due to slack and friction in the Bowden sheaths.

## V. DISCUSSION AND CONCLUSION

This paper presented the design and characterization of Elastic Spinners, a novel bidirectional torsional spring for rotary SEAs. The mechanism features dual output rotors enclosed within an input rotor assembly, interconnected by identical compression springs arranged circumferentially with minimal preload. Compared with state-of-the-art SEA torsional springs (Table. III), this configuration yields a compact form factor (outer diameter: 82 mm, thickness: 18.5 mm) with a linear stiffness response (43.8 Nm/rad) across a wide passive deflection range ($\pm$24 deg), while achieving high torque capacity (18 Nm) and low frictional losses (2.87%).

Elastic Spinners differs from conventional antagonistic designs, where motion in one direction compresses one set of springs while concurrently releasing the opposing set [17], [22]; such designs constrain passive deflection by the requirement that both sets of springs remain within their allowable deformation ranges. In contrast, all springs in Elastic Spinners deform in the same direction. This allows for a minimal preload that consumes only a small fraction of the available spring stroke, maximizing the remaining travel for passive deflection.

Elastic Spinners exhibited lower energy losses than those reported in [8], despite providing a passive deformation range more than 1.5 times greater than that design. A plausible explanation lies in the minimal sliding friction between the compression spring coils and their chambers, achieved through chamber designs incorporating sufficient clearance gaps and arc cutouts, which reduce coil–wall contact during compression. Furthermore, clearance gaps in the arc slots of the output rotors accommodate slight deviations from ideal circular arcs as the springs deform, preventing sliding between the coils and the output rotors. Additionally, each output rotor is seated against the extended inner ring of a bearing, ensuring axial clearance between the inner and outer rotors and substantially reducing frictional forces as the rotors rotate relative to one another. By contrast, the two-part cantilever design in [8] introduces sliding contacts between the outer rim and camshaft, resulting in more pronounced energy losses (5%).

The low friction and reduced rotor inertia of Elastic Spinners, combined with a gearless actuator and a cable loop realizing a moderate transmission ratio, contributed to excellent SEA dynamic performance. The torque bandwidth exceeded 8.4 Hz at 75% of torque capacity, demonstrating improved performance relative to existing SEA whose passive stiffness is within the same order of magnitude, such as the monolithic designs in [29] and [11], at both high (12 Nm) and moderate (6 Nm) torque amplitudes, despite the monolithic designs having higher passive stiffness (82 to 119 Nm/rad). Although higher bandwidth values have been reported in the SEA literature (e.g., 39.6 Hz for an elastic element based on linear tension springs in [20]), these designs are typically intended for low-torque applications and are therefore tested with smaller-amplitude chirp inputs (e.g., 1 Nm amplitude for the design in [20]).

The high bandwidth of this SEA makes it a strong candidate for pHRI applications. Bench testing demonstrated high fidelity in rendering virtual impedances across the feasible range $[0, K_{\mathrm{ES}}]$, while a preliminary treadmill-walking test with the SEA integrated into an ankle exoskeleton showed relatively small tracking errors (1.48 Nm RMSE) when exerting 98% of its torque capacity.

Future work will examine the performance of Elastic Spinners in multi-rotor configurations and with higher-stiffness linear compression springs. Both approaches are expected to enhance the torsional stiffness of the dual-rotor design

presented here, while maintaining its deformation range. In parallel, gait-training studies with healthy individuals are being carried out to assess the feasibility of new reinforcement learning-based pHRI controllers for the ankle exoskeleton used in this work, aimed at improving the wearer's walking speed [30], [31], while proof-of-concept trials in clinical populations are anticipated in the near future.

## REFERENCES


[1] N. Paine, J. S. Mehling, J. Holley, N. A. Radford, G. Johnson, C.-L. Fok, and L. Sentis, "Actuator control for the NASA-JSC valkyrie humanoid robot: A decoupled dynamics approach for torque control of series elastic robots," *Journal of field robotics*, vol. 32, no. 3, pp. 378–396, 2015.

[2] S.-S. Yoon, S. Kang, S.-J. Kim, Y.-H. Kim, M. Kim, and C.-W. Lee, "Safe arm with MR-based passive compliant joints and visco-elastic covering for service robot applications," in *Proceedings 2003 IEEE/RSJ International Conference on Intelligent Robots and Systems (IROS 2003)(Cat. No. 03CH37453)*, vol. 3. IEEE, 2003, pp. 2191–2196.

[3] S. Lee, S. Choi, C. Ko, T. Kim, and K. Kong, "Design and control of the compact cable-driven series elastic actuator module in soft wearable robot for ankle assistance," *International Journal of Control, Automation and Systems*, vol. 21, no. 5, pp. 1624–1633, 2023.

[4] B. Zhong, K. Guo, H. Yu, and M. Zhang, "Toward gait symmetry enhancement via a cable-driven exoskeleton powered by series elastic actuators," *IEEE robotics and automation letters*, vol. 7, no. 2, pp. 786–793, 2021.

[5] A. De Santis, B. Siciliano, A. De Luca, and A. Bicchi, "An atlas of physical human–robot interaction," *Mechanism and Machine Theory*, vol. 43, no. 3, pp. 253–270, 2008.

[6] G. Carpino, D. Accoto, F. Sergi, N. Luigi Tagliamonte, and E. Guglielmelli, "A novel compact torsional spring for series elastic actuators for assistive wearable robots," *Journal of Mechanical Design*, vol. 134, no. 12, p. 121002, 2012.

[7] A. Kuru, B. Ugurlu, and O. Bebek, "Design and development of a torsion-based series elastic actuator with nested encoders for a wearable exoskeleton robot," in *ACTUATOR 2022; International Conference and Exhibition on New Actuator Systems and Applications*. VDE, 2022, pp. 1–4.

[8] Z. Bons, G. C. Thomas, L. Mooney, and E. J. Rouse, "An energy-dense two-part torsion spring architecture and design tool," *IEEE/ASME Transactions on Mechatronics*, 2023.

[9] C. Lagoda, A. C. Schouten, A. H. Stienen, E. E. Hekman, and H. van der Kooij, "Design of an electric series elastic actuated joint for robotic gait rehabilitation training," in *2010 3rd IEEE RAS & EMBS international conference on biomedical robotics and biomechatronics*. IEEE, 2010, pp. 21–26.

[10] J. P. Cummings, D. Ruiken, E. L. Wilkinson, M. W. Lanighan, R. A. Grupen, and F. C. Sup IV, "A compact, modular series elastic actuator," *Journal of Mechanisms and Robotics*, vol. 8, no. 4, p. 041016, 2016.

[11] W. M. Dos Santos, G. A. Caurin, and A. A. Siqueira, "Design and control of an active knee orthosis driven by a rotary series elastic actuator," *Control Engineering Practice*, vol. 58, pp. 307–318, 2017.

[12] N. Georgiev and J. Burdick, "Design and analysis of planar rotary springs," in *2017 IEEE/RSJ International Conference on Intelligent Robots and Systems (IROS)*. IEEE, 2017, pp. 4777–4784.

[13] T. Kim, K. Shi, and K. Kong, "A compact transmitted-force-sensing series elastic actuator with optimized planar torsional spring for exoskeletons," in *2021 IEEE/ASME International Conference on Advanced Intelligent Mechatronics (AIM)*. IEEE, 2021, pp. 572–577.

[14] O. S. Al-Dahiree, R. A. R. Ghazilla, M. O. Tokhi, H. J. Yap, and M. Gul, "Design and characterization of a low-cost and efficient torsional spring for ES-RSEA," *Sensors*, vol. 23, no. 7, p. 3705, 2023.

[15] A. H. Stienen, E. E. Hekman, H. Ter Braak, A. M. Aalsma, F. C. Van Der Helm, and H. Van Der Kooij, "Design of a rotational hydroelastic actuator for a powered exoskeleton for upper limb rehabilitation," *IEEE Transactions on biomedical engineering*, vol. 57, no. 3, pp. 728–735, 2009.

[16] S. Wang, C. Meijneke, and H. van der Kooij, "Modeling, design, and optimization of mindwalker series elastic joint," in *2013 IEEE 13th International Conference on Rehabilitation Robotics (ICORR)*. IEEE, 2013, pp. 1–8.

[17] N. G. Tsagarakis, M. Laffranchi, B. Vanderborght, and D. G. Caldwell, "A compact soft actuator unit for small scale human friendly robots," in *2009 IEEE international conference on robotics and automation*. IEEE, 2009, pp. 4356–4362.

[18] H. Toubar, M. I. Awad, M. N. Boushaki, Z. Niu, K. Khalaf, and I. Hussain, "Design, modeling, and control of a series elastic actuator with discretely adjustable stiffness (SEADAS)," *Mechatronics*, vol. 86, p. 102863, 2022.

[19] J. Song, A. Zhu, Y. Tu, X. Zhang, and G. Cao, "Novel design and control of a crank-slider series elastic actuated knee exoskeleton for compliant human–robot interaction," *IEEE/ASME Transactions on Mechatronics*, vol. 28, no. 1, pp. 531–542, 2022.

[20] L. Tiseni, G. Rinaldi, D. Chiaradia, and A. Frisoli, "Design and control of a linear springs-based rotary series elastic actuator for portable assistive exoskeletons," in *2021 30th IEEE International Conference on Robot & Human Interactive Communication (RO-MAN)*. IEEE, 2021, pp. 434–439.

[21] W. Zhao, J. Liao, W. Qian, H. Yu, and Z. Guo, "A novel design of series elastic actuator using tensile springs array," *Mechanism and Machine Theory*, vol. 192, p. 105541, 2024.

[22] M. Lv, W. Chen, X. Ding, J. Wang, and X. Chen, "A new designed quadruped robot with elastic joints," in *2014 IEEE International Conference on Automation Science and Engineering (CASE)*. IEEE, 2014, pp. 1002–1007.

[23] D. A. Winter, *Biomechanics and motor control of human gait*. Waterloo, Ontario: Univ. of Waterloo Press, 1991.

[24] T. Chen, Z. Lu, and C. Su, "Analysis method for elastic characteristics of arc spring," *China Mech Eng*, vol. 17, no. 5, pp. 493–495, 2006.

[25] A. M. Wahl, *Mechanical springs*. Waterloo, Ontario: Mcgraw-Hill Book Company, 1963.

[26] M. T. Eraky, A. Li, M. H. Rocha, A. Teker, B. A. Gebre, K. J. Nolan, K. Pochiraju, and D. Zanotto, "A novel personalized ankle exoskeleton with co-located SEA for gait training," in *2024 10th IEEE RAS/EMBS Int. Conf. Biomed. Robot. Biomechatron. (BioRob)*, 2024, pp. 1715–1720.

[27] Y. Zhang, S. Li, K. J. Nolan, and D. Zanotto, "Shaping individualized impedance landscapes for gait training via reinforcement learning," *IEEE Transactionsx on Medical Robotics and Bionics*, vol. 4, no. 1, pp. 194–205, 2021.

[28] J. E. Colgate and J. M. Brown, "Factors affecting the z-width of a haptic display," in *Proceedings of the 1994 IEEE International Conference on Robotics and Automation*. IEEE, 1994, pp. 3205–3210.

[29] F. Sergi, D. Accoto, G. Carpino, N. L. Tagliamonte, and E. Guglielmelli, "Design and characterization of a compact rotary series elastic actuator for knee assistance during overground walking," in *2012 4th IEEE RAS & EMBS international conference on biomedical robotics and biomechatronics (BioRob)*. IEEE, 2012, pp. 1931–1936.

[30] A. Li, H. Li, A. Teker, M. H. Rocha, B. A. Gebre, K. J. Nolan, K. Pochiraju, and D. Zanotto, "Reinforcement learning assist-as-needed control promotes recovery of walking speed following ankle weight perturbations," in *2025 IEEE/RSJ Int. Conf. Intell. Robots Syst. (IROS)*, 2025, pp. 46–51.

[31] ——, "Reinforcement learning control outperforms iterative learning in exoskeleton-assisted gait training," in *2026 Int. Conf. Robot. Autom. (ICRA)*, 2026.